

Theory for strength and stability of an unusual “ligand-receptor” bond: a microtubule attached to a wall by molecular motor tethers

Dipanwita Ghanti and Debashish Chowdhury^a

Department of Physics, Indian Institute of Technology Kanpur, 208016, India

A microtubule (MT) is a tubular stiff filament formed by a hierarchical organization of tubulin proteins. We develop a stochastic kinetic model for studying the strength and stability of a pre-formed attachment of a MT with a rigid wall where the MT is tethered to the wall by a group of motor proteins. Such an attachment, formed by the specific interactions between the MT and the motors, is an analog of ligand-receptor bonds; the MT and the motors anchored on the wall being the counterparts of the ligand and receptors, respectively. However, unlike other ligands, the length of a MT can change with time because of its polymerization-depolymerization kinetics. The simple model developed here is motivated by the MTs linked to the cell cortex by dynein motors. We present the theory for both force-ramp and force-clamp conditions. In the force-ramp protocol we investigate the strength of the attachment by assuming imposition of a time-dependent external load tension that increases linearly with time till the attachment gets ruptured; we calculate the distribution of the rupture forces that fluctuates from one loading to another. In the force-clamp protocol, to test the stability, we compute the distribution of the lifetimes of the attachments under externally applied time-independent load tension; the results establish the MT-wall attachment to be an analog of a slip-bond.

arXiv:1610.04835v1 [q-bio.SC] 16 Oct 2016

^a Corresponding author; e-mail: debch@iitk.ac.in

I. INTRODUCTION

The structure, strength and stability of ligand-receptor bonds have been investigated extensively over several decades [1]. The concepts (and definitions) of ligand and receptor have also evolved during this period. In the words of Martin Karplus [2], “the ligand can be as small as an electron, an atom or diatomic molecule and as large as a protein”. In principle, the definition of a ligand can be extended even further to a stiff filament formed by a hierarchical organization of proteins; the microtubule (MT) [3], a nano-tube in eukaryotic cells, is an example of such filaments. Thus, if such a stiff straight filament is tethered to a flat rigid wall by wall-anchored proteins that bind specifically to the filament, the attachment can be viewed as a ‘ligand-receptor bond’ where the filament is the analog of a ligand. Inspired by this generalized definition of ligands and receptors, we study here a very special type of *non-covalent* filament-wall attachment from the perspective of ligand-receptor bonds. The tether protein that we consider here are ‘active’ in the sense that these consume chemical fuel for their mechanical function.

The theoretical model developed in this paper is motivated by the typical attachment formed by a MT with the cortex of a living eukaryotic cell where the two are linked by dynein molecules [4]; dynein is a motor protein powered by input chemical energy extracted from ATP hydrolysis [5, 6]. There are equispaced dynein-binding sites on the surface of a MT where the head of a dynein can bind specifically; the tail of the dyneins are anchored on the cortex. Thus, dyneins function as tethers linking the MT with the wall; unbinding of *all* the dynein heads from the MT would rupture the MT-cortex attachment. However, the model developed in this paper captures only some of the key features of the real MT-cortex attachments like, for example, the polymerization-depolymerization of MT [7]. The wall in our model mimics the cell cortex. It is worth pointing out that the MT-wall model developed here differs fundamentally from another MT-wall model reported earlier in ref.[8] (from now onwards referred to as the SSC model). Unlike the active (i.e., energy consuming) linkers, which here mimic dynein motors, the dominant tethers in the SSC model are passive. Moreover, the wall in the SSC model represents a kinetochore [9], a proteinous complex on the surface of a chromosome, whereas the wall in the model developed in this paper represents the cell cortex.

Although the formation of the MT-wall attachment itself is an interesting phenomenon, we do not study it here. Instead, in this paper we consider a pre-formed attachment to investigate its strength and stability using a kinetic model that mimics the protocols of dynamic force spectroscopy [10, 11]. Two distinct protocols are routinely used in force spectroscopy for measuring the strength and stability of ligand-receptor bonds [1]. In the *force-clamp* protocol, a time-independent load tension is applied against the bond; the time duration after which the bond is just broken is the life time of the bond. Since the underlying physical process is dominated by thermal fluctuations different values of life time are observed upon repetition of the experiment. Therefore, the *stability* of the bond is characterized by the life time distribution (LTD). On the other hand, in the *force-ramp* protocol the magnitude of the time-dependent load tension is ramped up at a pre-decided rate till the bond just gets ruptured; the rupture force distribution (RFD) characterizes the *strength* of the bond. For a *slip-bond* the mean life time (MLT) decreases monotonically with the increasing magnitude of the tension in the force-clamp experiment. In contrast, a nonmonotonic variation (an initial increase followed by decrease) of the MLT with increasing load tension in the force-clamp experiments is a characteristic feature of *catch-bonds* [12, 13]. Although the force-ramp is a more natural protocol for dynamic force spectroscopy [10] the results provide somewhat indirect evidence for catch-bonds.

We mimic both the force-clamp and force-ramp protocols in our computer simulations of the theoretical model to compute the LTD and RFD for the motor-linked MT-wall attachment. The results establish that this attachment is, effectively, like a slip-bond. This is in sharp contrast to results obtained from the SSC model; the latter exhibits a catch-bond-like behavior as observed also in experiments performed *in-vitro*. To our knowledge, similar dynamic force spectroscopic experiments have not been attempted so far on MT-cell cortex attachments. Nevertheless, our generic theoretical model and the results are likely to motivate such experiments in near future. The model is quite general. In principle, the same model can serve, after appropriate minor adaptation, as a minimal model for many other attachments formed by a polymerizing-depolymerizing filament with a wall where the specific interaction of the two arises from a set of active linkers.

II. MODEL

We model the MT as a strictly one-dimensional stiff filament. The plus end of the MT is oriented along the +X-direction of the one-dimensional coordinate system chosen for the model. The rigid wall facing the MT filament is perpendicular to the X-axis. As stated earlier, our model is motivated by the cortex-MT attachment where dynein motors tether the MT to the cortex. Since a dynein motor, fuelled by ATP, has a natural tendency to walk towards the minus end of the MT, the molecular motors in our model are also assumed to be minus-end directed, while consuming input energy, in the absence of external load tension. We assume that each motor is permanently anchored onto the rigid wall and cannot detach from it while the head of a motor can attach to the MT and a motor already

attached to the MT can also detach from it. We model the linkage between a motor and the rigid wall by an elastic element that is approximated as a Hookean spring. The wall is assumed to execute one-dimensional diffusion along the X-coordinate with a diffusion constant D .

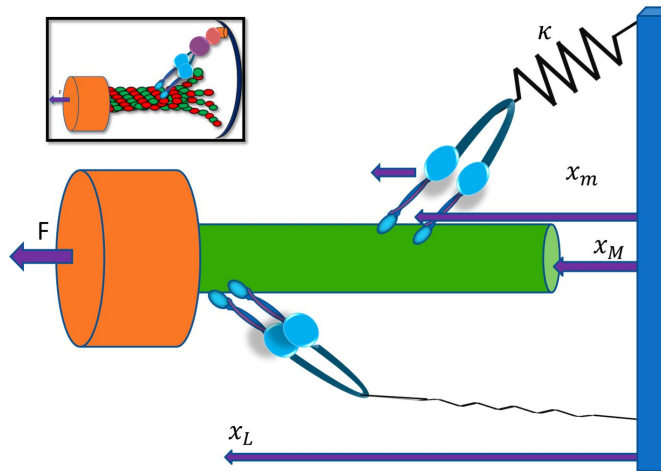


FIG. 1. Cartoon of a dynein motor attached with cell cortex (blue wall). x_M and x_m represents the distance of MT tip and dynein motor from cell cortex. In the inset MT interact with cell cortex through the cortical dynein motor and dynein motor is attached with cell cortex using different protein. Dynein are attached with cell cortex through a spring with spring constant k . External Force F is applied on axoneme (orange) from which MTs (green) are generated.

Although each dynein motor has two heads, each capable of binding specific sites on the MT, we denote the position of a motor by the location of its midpoint. The two heads are, effectively, connected at the midpoint by a hinge; the midpoint is also linked to the point of anchoring on the wall by an elastic element that is assumed to be a Hookean spring. In the one-dimensional coordinate system the origin is fixed on the wall. With respect to this origin $x_m(t)$ denotes the position of the *midpoint* of an arbitrary molecular motor at time t while $x_M(t)$ denotes the corresponding position the MT tip. In this model, x_m can change because of the following processes:

- (i) stepping of a motor while the wall remains frozen in its current position, and
- (ii) diffusion of the wall while motor does not step out of its current binding site on the MT.

We assume that x_L is the maximum distance upto which a motor can bind to the MT. So the motor can bind only if its head is located between $x_M(t)$ and x_L (i.e., $x_M \leq x_m \leq x_L$). N_d is the total number of motors (the subscript 'd' indicates minus-ended directed motor like, for example, dynein) that can simultaneously attach to the MT whereas $n(t)$ denotes the number of motors actually attached at any arbitrary instant of time (i.e., $n(t) \leq N_d$). For any given unbound motor, \mathcal{K}_{on} denotes the rate of binding of its head to the MT. Therefore, at any arbitrary instant of time t , the rate of a binding event, i.e., the rate at which any of the unbound motor binds to the MT is [14]

$$k_{on}(n) = (N_d - n)\mathcal{K}_{on} \quad (1)$$

Because of being anchored on the fixed rigid wall, the motors bound to the MT cannot walk freely along the MT track. Moreover, because of the upper cutoff imposed on the maximum possible elongation of the spring, a motor can move only upto a maximum distance x_L . If the rest position of motor head is x_{m0} , the spring force acting on the motor is given by

$$F_{sp}(x_m) = k(x_m - x_{m0}) \quad (2)$$

Here we assume external load F to be equally shared by $n(t)$ motors so that each motor feels the load

$$F_{ex} = F/n(t). \quad (3)$$

Thus, the effective force felt by single motor head that is bound to MT and located at a position x_m is

$$F_{ef} = F_{ex} - F_{sp}. \quad (4)$$

where F_{sp} is given by (2).

Let $k_{off}(0)$ denote the rate of unbinding of the head of a motor in the absence of load force. When a load force F tends to rupture the attachment, the unbinding rate increases. Following Kramers (or Bell) theory we assume an approximate exponential dependence [15, 16]

$$k_{off}(F) = k_{off}(0)e^{F/F_d} \quad (5)$$

The characteristic ‘detachment force’ F_d can be expressed as $F_d = k_B T/x_d$ where x_d is the extension of the energy barrier between the bound and unbound state of a motor. The effective rate of unbinding of a single motor head from the MT is given by [14]

$$k_{off}(F_{eff}, n) = nk_{off}(0)e^{F_{eff}/F_d} \quad (6)$$

Suppose the rate of forward hopping of a motor towards the minus end of of the MT is k_{f0} . But the forward stepping of motor will be opposed by the spring force F_{sp} . Therefore, the effective rate of forward stepping of a motor is given by

$$k_f(F_{sp}) = k_{f0}e^{-F_{sp}\gamma/F_{sp}^*} \quad (7)$$

Here γ is a constant parameter ($0 < \gamma < 1$). The characteristic force F_{sp}^* can be expressed as $k_B T/\ell$ where ℓ is the length of a single subunit of MT. Based on the well known experimentally observed facts, we assume that a motor can also step towards the positive end of MT under sufficiently high load force [17–19]; the rate of stepping in that ‘reverse’ direction is given by

$$k_r(F_{sp}) = k_{r0}e^{F_{sp}(1-\gamma)/F_{sp}^*} \quad (8)$$

where the rate k_{r0} of stepping of a motor towards the plus end of the MT in the absence of load force is very small ($k_{r0} \ll k_{f0}$) because the natural direction of these motors is the minus end of MT. The form (8) captures the intuitive expectation that $k_r(F_{sp})$ would increase with increasing spring force.

The probability that (the midpoint of) a motor is located at x_m and MT tip is at x_M , while the total number $n(t)$ of motors are bound to the MT simultaneously at that instant of time, is given by $P_n(x_m, x_M, t)$. Note that x_M is a continuous variable whereas n can take only non-negative integer values. Let $P(x_m|y_m)$ be the conditional probability that, given a MT-bound motor located at site x_m , there is another MT-bound motor at site y_m on the MT ($x_M < x_m, y_m < x_L$). Then $\xi(x_m|y_m) = 1 - P(x_m|y_m)$ is the conditional probability that, given a motor at site x_m , the site y_m is empty. Let $\xi(x_m)$ be the probability that site x_m is not occupied by any motor, irrespective of the state of occupation of any other site.

Under MFA, the equations governing the time evolution of $P_n(x_m, x_M t)$ is given by

$$\begin{aligned} \frac{dP_n(x_m, x_M, t)}{dt} = & D \underbrace{\frac{\partial^2 P_n(x_m, x_M, t)}{\partial x_M^2}}_{\text{Diffusion of wall}} - \underbrace{v_F \frac{\partial P_n(x_m, x_M, t)}{\partial x_M}}_{\text{Drift velocity of MT tip}} \\ & \underbrace{k_f(F_{sp})P_n(x_m - 1, x_M, t)\xi(x_m - 1|x_m) - k_f(F_{sp})P_n(x_m, x_M, t)\xi(x_m|x_m + 1)}_{\text{Forward stepping of the motor if target site is empty}} \\ & + \underbrace{k_r(F_{sp})P_n(x_m + 1, x_M, t)\xi(x_m + 1|x_m) - k_r(F_{sp})P_n(x_m, x_M, t)\xi(x_m|x_m - 1)}_{\text{Reverse stepping of the motor if target site is empty}} \\ & + \underbrace{k_{on}(n - 1)(1 - P_{n-1}(x_m, x_M, t)) - k_{on}(n)(1 - P_n(x_m, x_M, t))}_{\text{Binding of motor to an empty site on MT}} \\ & + \underbrace{k_{off}(f_{eff}, n + 1)P_{n+1}(x_m, x_M, t) - k_{off}(f_{eff}, n)P_n(x_m, x_M, t)}_{\text{Unbinding of motor from an occupied site on MT}} \end{aligned} \quad (9)$$

where

$$v_F = \frac{F - \sum_{x_m=x_M}^{x_L} F_{sp}(x_m)}{\Gamma} + (\beta - \alpha)\ell \quad (10)$$

and ℓ , the length of each subunit of MT is also the spacing between the successive motor-binding sites on the MT. The rates of polymerization and de-polymerization of a MT tip are given by α and β , respectively.

Parameter	Values
Spacing between binding sites on MT ℓ	8/13 nm
Maximal distance dynein can bind x_L	32 nm
Rate of polymerization of MT α	30 s^{-1}
rate of Load-free depolymerization of MT β_0	350 s^{-1}
Rate of Binding of motor to MT k_{on}	3 s^{-1}
rate of Unbinding of motor from MT $k_{off}(0)$	3 s^{-1}
rate of Forward stepping of motor k_{f0}	6 s^{-1}
rate of Backward stepping of motor $k_{r0}(0)$	0.1 s^{-1}
Characteristic depolymerization force F_\star	1 pN
Characteristic spring force of motor $F_{sp\star}$	1 pN
Rest length of the spring x_{m0}	10 nm
Spring constant k	1000 $pN\mu m^{-1}$
Diffusion constant D	700 $nm^2 s^{-1}$
Effective drag coefficient Γ	6 $pNs\mu^{-1}$

TABLE I. Numerical values of the parameters used in simulations.

The rate of depolymerization of MT is suppressed by externally applied tension [20]. We assume that the MT-bound minus-end directed motors at the tip (plus-end) of the MT prevents MT protofilaments from curling outwards, thereby slowing down depolymerization rate [21]:

$$\beta = \beta_0 \exp\left(-[F_{sp}(x_m = x_M) - F_{ex}\delta_{x_m, x_M}]/F_\star\right). \quad (11)$$

where F_\star is the characteristic load force at which the MT depolymerization rate is an exponentially small fraction of β_0 . The Kronecker delta function ensures that the external force affects the depolymerization rate β only if the motor is bound to the tip of the MT.

The force balance equation is given by

$$\frac{dx_M(t)}{dt} = \frac{F - \sum_{x_m=x_M}^{x_L} F_{sp}(x_m)}{\Gamma} + (\beta - \alpha)\ell + \frac{\eta(t)}{\Gamma} \quad (12)$$

where $\eta(t)$ is a Gaussian white noise. Let $Q(x_M, t)$ be the probability of finding MT tip at position x_M at time t . Time evolution of the $Q(x_M, t)$ govern by the Fokker-Planck equation

$$\frac{dQ(x_M, t)}{dt} = D \frac{\partial^2 Q(x_M, t)}{\partial x_M^2} - v_F \frac{\partial Q(x_M, t)}{\partial x_M} \quad (13)$$

This Fokker-Planck equation can also be re-cast as an equation of continuity for the probability density $Q(x_M, t)$ with the probability current density $J(x_M, t)$ which is given by

$$J(x_M, t) = -D \left[\frac{\partial Q(x_M, t)}{\partial x_M} + \frac{U'}{k_B T} Q(x_M, t) \right]. \quad (14)$$

For the calculation of the lifetime of the MT-wall attachment, we have assumed that initially there is no gap between MT tip and cell wall i.e $Q(x_M, t=0) = \delta(x_M)$. We have imposed reflecting boundary at the cell wall because MT tip cannot penetrate the cell wall. So

$$J(x_M = 0, t) = \left(\frac{\partial Q(x_M, t)}{\partial x_M} - \frac{v_F}{D} Q(x_M) \right)_{x_M=0} = 0 \quad (15)$$

We have placed an absorbing boundary at $x_M = x_L$ so that $Q(x_M = x_L, t) = 0$; this boundary condition is motivated by our calculation of the life time of the MT-wall attachment where the lifetime is essentially a first-passage time [22–25].

III. SIMULATION

By using a method of discretization proposed originally by Wang, Peskin and Elston [26, 27], we discretize space into contiguous discrete cells, each of length h , where x_j denotes the position of the center of the j -th cell. The potential

$U(x)$ is thus replaced by the discretized counterpart

$$\frac{U_j}{k_B T} = \left[\frac{F - \sum_{x_m=x_M}^{x_L} F_{sp}(x_m)}{\Gamma} + \ell \frac{(\beta - \alpha)}{D} \right] x_j \quad (16)$$

Because of this discretization, the Fokker-Planck equation (13) is replaced a master equation where the discrete jumps from the center of one cell to those of its adjacent cells in the forward or backward directions are given by the transition rates

$$w_f(j) = \frac{D}{h^2} \frac{\frac{-\delta U_j}{k_B T}}{\exp(\frac{-\delta U_j}{k_B T}) - 1} \quad (17)$$

and

$$w_b(j) = \frac{D}{h^2} \frac{\frac{\delta U_j}{k_B T}}{\exp(\frac{\delta U_j}{k_B T}) - 1}, \quad (18)$$

respectively, where $\delta U_j = U_{j+1} - U_j$. We have carried out simulations of this discretized version of the model using Gillespie algorithm [28]. In each time step Δt six types of event are possible, namely, binding/ unbinding, forward/backward hopping of each motor and forward/backward movement of the MT tip. In the simulation a motor can attach to a site x_j only if it is empty. Similarly, a motor can step forward or backward provided the target site is empty. We have generated trajectories up to 10^6 time steps and, after averaging over the trajectories we get the results of our interest. The common parameter values used in the simulation are listed in table I.

IV. RESULTS

In the two subsections we present the results of our simulations under force-clamp and force-ramp conditions. The main quantities of interest in these two cases are the LTD and RFD, respectively.

A. Force clamp condition

In the Fig.2(a) the probability distributions of the lifetimes are plotted for three different fixed values of the externally applied tension F . The corresponding values of the mean lifetimes τ are plotted against F in Fig.2(b).

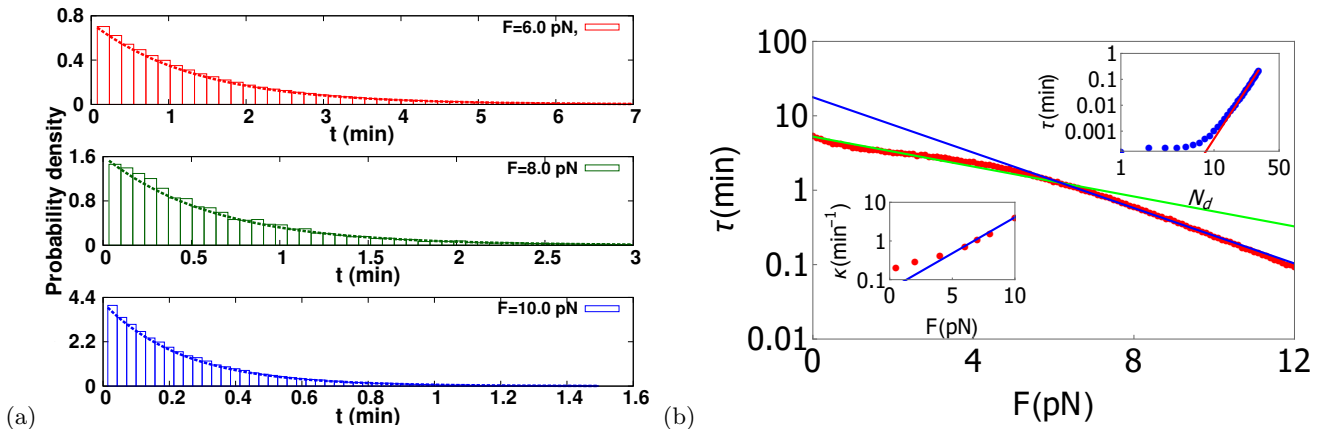


FIG. 2. (a) Probability distributions of the lifetimes are plotted in the three panels (from top to bottom) for different applied tension, namely, $F = 6pN$ (red) $F = 8pN$ (green) and $F = 10pN$ (blue). (b) Semi-log plot of the mean lifetime τ of the attachment against the applied external tension F for fixed $N_d = 10$. The dependence of the mean life time τ on the number of motors N_d is shown by the log-log plot in the inset (upper right corner of (b)) for a fixed of tension $F = 30pN$. The dependence of κ on F is displayed by the semi-log plot in the second inset (lower left corner of (b)). All the lines represent analytical functions that have been fitted to the numerical data that were obtained from computer simulation and are plotted with discrete points (please see the text for the details of the fitting procedure).

Each of the distributions of lifetimes shown in the three panels of Fig.2(a), for which F has a fixed value, has been fitted to the function (see the lines fitted to the data) [11, 29]

$$P(t) = \kappa(F)\exp\left(-\kappa(F)t\right) \quad (19)$$

to extract the numerical value of the fitting parameter κ which has a dimension of time^{-1} . By repeating this fitting process also for several other values of F (for which the distributions of the lifetimes have not been presented in this paper), we have extracted the F -dependence of the fitting parameter κ . The “best fit function” $\kappa(F)$ is plotted in the inset in the lower left corner of Fig.2(b). The function $\kappa(F)$, in turn, is well approximated by the functional form [11, 29]

$$\kappa(F) = \kappa(0)\exp(F/F_0) \quad (20)$$

with $\kappa(0) \simeq 0.056 \text{ min}^{-1}$ and $F_0 \simeq 2.33 \text{ pN}$.

The monotonic decrease of the mean lifetime τ with F indicates a slip-bond-like behaviour of the MT-motor attachment. Moreover, the best fits (19) and (20) would suggest a functional form [11, 29]

$$\tau(F) = \frac{1}{\kappa(F)} = \frac{1}{\kappa(0)}e^{-F/F_0}. \quad (21)$$

The simulation data for $\tau(F)$ corresponding to $F > 6 \text{ pN}$, indeed, fit well with the form (21), if the values $\kappa(0) \simeq 0.056 \text{ min}^{-1}$ and $F_0 \simeq 2.33 \text{ pN}$ extracted above from Fig.2(a) are used (see the blue line fit in Fig.2(b)). But, for $F < 6 \text{ pN}$, this fit shows increasing deviation from the simulation data with decreasing F . However, in the regime $F < 6 \text{ pN}$, the functional form (21) would still be consistent with the numerical data for τ if one uses $\kappa(0) \simeq 0.19 \text{ min}^{-1}$ and $F_0 \simeq 4.32 \text{ pN}$ for the two fitting parameters (see the green dashed line in Fig.2(b)). Thus, the simulation data indicate two different regimes in both of which τ decreases exponentially with F , but the decrease is sharper in the higher tension regime that corresponds to $F > 6 \text{ pN}$. A possible interpretation of these two apparent regimes is that in the exponential of the expression for $\kappa(F)$ there is a correction term proportional to F^2 ; such corrections emerge naturally from systematic Taylor expansion in the extended Bell models [30, 31].

From the log-log plot of τ against N_d in the inset at the upper right corner of the Fig.2(b) we conclude that the mean lifetime increases nonlinearly with the number of motors following

$$\tau \propto N_d^\nu, \quad (22)$$

with $\nu \simeq 5.5$. The effects of the motors on the lifetime of the MT-surface attachment is not simply additive. Recall that, at any arbitrary instant of time t , the load force is equally shared by the $n(t)$ number of motors bound to the MT. Therefore, unbinding of a motor from the MT increases the load on those still attached to it. If the redistributed share of the load is too high to resist, more motors are likely to unbind from the MT thereby causing further increase in the load share of the remaining motors still bound to the MT. The larger is the total number N_d , less catastrophic is the effect of such “avalanche” of unbinding of the motors and hence the nonlinear increase in the mean lifetime of the MT-wall attachment.

B. Force ramp condition

The distribution of the rupture force obtained from our simulation using the ramp force $F(t) = at$ is shown in the Fig.3(a). At any constant loading rate, the distribution exhibits a single peak; the asymmetric bell-shape is the well known typical shape of RFD for common ligand-receptor bonds[11]. At very small forces the bonds are unlikely to get enough time to rupture. Similarly, at very large forces the likelihood of bond rupture is also small because the bond would have ruptured already at some intermediate value of the force. Therefore, $\rho(F)$ is expected to be small at both the extremes; naturally, it would exhibit a peak corresponding to some intermediate value of force. These intuitive arguments not only explain the qualitative shape of $\rho(F)$ in Fig.3(a) but also the observation that most probable rupture force (i.e., the force that corresponds to the peak in the distribution of the rupture forces) is larger in case of a faster loading rate.

The simulation data fits well with the function [11, 29]

$$\rho(F) = \frac{c\kappa(F)}{a} \exp\left[-\frac{c}{a} \int_0^F \kappa(F')dF'\right] \quad (23)$$

with a dimensionless fitting parameter $c \simeq 0.017$ and $\kappa(F) = 1/\tau(F)$, given by (20).

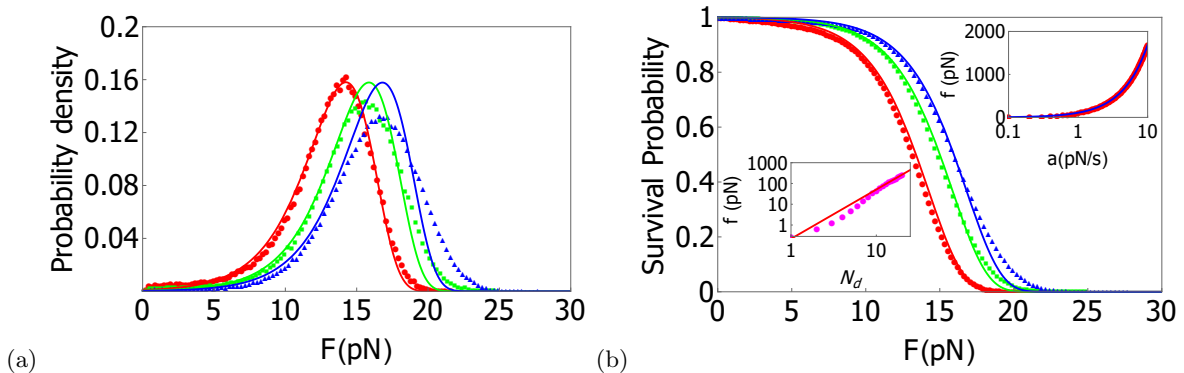


FIG. 3. (a) Probability distributions of the rupture force are plotted for three different loading rates, namely, $a = 1pNs^{-1}$ (red line and circles), $a = 2pNs^{-1}$ (green line and squares) and $a = 3pNs^{-1}$ (blue line and triangles). (b) The survival probability for the three different loading rates $a = 1pNs^{-1}$ (red line and circles), $a = 2pNs^{-1}$ (green line and squares) and $a = 3pNs^{-1}$ (blue line and triangles) are plotted against the tension F . The mean rupture force f is plotted against the loading rate a (blue line and red circles) in the inset at the upper right corner of (b). The dependence of the mean rupture force f on the number of motors N_d is displayed (red line and magenta circles) in the inset at the lower left corner of (b). In all the figure lines represent the best fits to the simulation data (please see the text for the details of the fitting procedure)

The survival probability $S(t)$ is defined as the probability that till time t the MT tip has not reached the absorbing boundary at x_L . As is well known [29], the survival probability $S(F(t))$ is related to the detachment rate $\kappa(F)$ by [11, 29]

$$S(F) = \exp \left[-\frac{1}{a} \int_0^F \kappa(F') dF' \right] \quad (24)$$

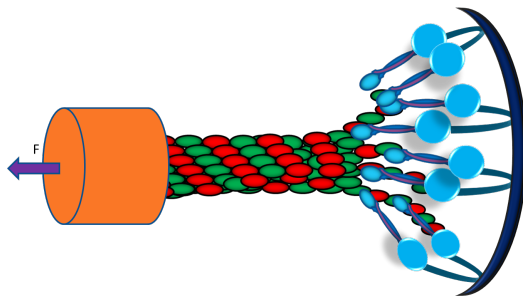


FIG. 4. A schematic description of a the typical experimental set up proposed to test the qualitative features of the results obtained from our generic model. The plus end of single MT is linked with the cell cortex by dynein motors and an external load tension F is applied on a suitable handle (orange cylinder) attached to the minus end of the same MT.

In the Fig.3(b) the simulation data for the survival probability are compared with the corresponding function $S(F)$ obtained using (24). The agreement is excellent thereby establishing consistency of the data obtained for the different quantities from our computer simulations. As expected $S(t) = 1$ at $t = 0$ (i.e., $F = 0$) and $S(t) \rightarrow 0$ as $t \rightarrow \infty$ (i.e., $F \rightarrow \infty$). The survival probability remains high upto certain force after which it falls rapidly. It is worth pointing out that one can account for the skewed shape of the curves $\rho(F)$ in Fig.3(a) mathematically [11] exploiting increase of $\kappa(F)$ and sharp decrease of $S(F)$ in the relation $\rho(F) \propto \kappa(F)S(F)$.

V. SUMMARY AND CONCLUSION

Extending the earlier generalizations [2] of the concept of a ligand, we have treated a microtubule (MT) as a ‘ligand’ that is tethered to a ‘receptor’ wall by a group of minus-end directed molecular motors [5]. The tails of the motors are permanently anchored on the wall while their motor heads can bind to- and unbind from the MT. This model of MT-wall attachment captures only a few key ingredients of the MT-cortex attachments in eukaryotic cells, particularly those formed during chromosome segregation. This minimal model incorporates the polymerization and depolymerization kinetics of MT. But, for the sake of simplicity, it does not include the processes of ‘catastrophe’ and ‘rescue’ that are caused by the ‘dynamic instability of MT filaments’ citedesai97 although these can be captured in an extended version of this model [32]. We consider a pre-formed MT-wall attachment and carry out computer simulations to study statistical properties of its rupture under conditions that mimic the protocols of force-clamp and force-ramp experiments *in-vitro* [10, 11]. The simulation results that we report are interpreted in the light of the theory of single-molecule force spectroscopy, popularized by Bell [15] and some of its later generalizations [11].

To our knowledge, the *in-vitro* experimental set up (schematically depicted in Fig.4) that comes closest to our model is that used by Laan et al. [21]; the wall in our model corresponds to the microfabricated vertical barrier that mimics the cell cortex in their experiment. Dynein motors were anchored on the barrier just as we have depicted in Fig.1 for our model. In the experiment these dyneins captured the MT that grew from a centrosome which was fixed on a horizontal glass surface. A slightly different *in-vitro* experimental set up was used by Hendricks et al. [33]; in this experiment a dynein coated bead was used to mimic the cell cortex. However, within the broader context of the role of MT-cortex interaction in positioning of the mitotic spindle, the authors of refs.[21, 33], demonstrated only the stabilization of the MT by the dynein tethers. In contrast, the main aim of our study is to focus on the LTD and RFD for the pre-formed attachment of a MT with a wall tethered by minus-end directed motors.

ACKNOWLEDGMENTS

This work has been supported by a J.C. Bose National Fellowship (DC) and by the “Prof. S. Sampath Chair” Professorship (DC).

-
- [1] P. Bongrand, Rep. Prog. Phys. **62**, 921 (1999).
 - [2] M. Karplus, J. Mol. Recognit. **23**, 102 (2010).
 - [3] J.D. Lawson and R.E. Carazo Salas, Biochem. Soc. Trans. **41**, 1736 (2013).
 - [4] H. Tuncay and K. Ebnet, Cell. Mol. Life Sci. **73**, 1195 (2016).
 - [5] D. Chowdhury, Phys. Rep. **529**, 1 (2013).
 - [6] A.B. Kolomeisky, *Motor proteins and Molecular Motors*, (CRC Press, 2015).
 - [7] A. Desai and T.J. Mitchison, Annu. Rev. Cell Dev. Biol. **13**, 83 (1997).
 - [8] A. K. Sharma, B. Shtylla and D. Chowdhury, Phys. Biol. **11**, 1478 (2014).
 - [9] I. M. Cheeseman and A. Desai, Nat. Rev. Mol. Cell. Biol. **9**, 33 (2008).
 - [10] A.R. Bizzarri and S. Cannistraro (eds.) *Dynamic Force Spectroscopy and Biomolecular Recognition*, (CRC Press, 2012).
 - [11] G. Arya, Molecular Simulation, **42**, 1102 (2016).
 - [12] W. E. Thomas, Annu. Rev. Biomed. Eng. **10**, 39 (2008).
 - [13] W. E. Thomas, V. Vogel and E. Sokurenko, Annu. Rev. Biophys. **37**, 399 (2008).
 - [14] M. Muller, S. Klumpp, and R Lipowsky, PNAS. **105**, 4609, (2008).
 - [15] G.I. Bell. Science, **200**, 618, (1978).
 - [16] H.A. Kramers. Physica, **7**, 284,(1940).
 - [17] R. Mallik, B.C. Carter, S.A. Lex, S.J. King, and S.P. Gross. Nature, **427**, 649, (2004).
 - [18] S.L. Reck-Peterson, A. Yildiz, A.P. Carter, A. Gennerich, N. Zhang, and R.D. Vale. Cell, **126**, 335, (2006).
 - [19] S. Toba, T.M. Watanabe, L. Yamaguchi-Okimoto, Y.Y. Toyoshima, and H. Higuchi. Proc. Natl. Acad. Sci. USA, **103**, 5741, (2006).

- [20] A. D. Franck, A. F. Powers, D. R. Gestaut, T. Gonen, T. N. Davis, C. L. Asbury, *Nat Cell Biol* **9**, 832 (2007).
- [21] L. Laan, S. Roth, M. Dogterom, *Cell Cycle* **11**, 3750 (2012).
- [22] S. Redner, *A Guide to First-Passage Processes* (Cambridge University Press, Cambridge, 2001)
- [23] S. Redner, R. Metzler and G. Oshanin, (eds) *First-passage Phenomena and their Applications*, (World Scientific Publishing Co., 2014).
- [24] S. Iyer-Biswas and A. Zilman, *Adv. Chem. Phys.* **160**, 261 (2016).
- [25] N. Polizzi, M.J. Therien, D.N. Beratan, *Israel J. Chem.* (2016).
- [26] H. Wang, C. Peskin and T. Elston, *J. Theo. Biol.* **221**, 491 (2003).
- [27] H. Wang, T. C. Elston, *J. Stat. Phys.* **128**, 35 (2007).
- [28] D.T. Gillespie, *Annu. Rev. Phys. Chem.* **58**, 35(2007).
- [29] R. W. Friddle, in: [10].
- [30] D.E. Makarov, *J. Chem. Phys.* **144**, 030901 (2016).
- [31] S.S.M. Konda, J.N. Brantley, C.W. Bielawski and D.E. Makarov, *J. Chem. Phys.* **135**, 164103 (2011).
- [32] D. Ghanti, Ph.D. Thesis, IIT Kanpur (2016) (in preparation).
- [33] A.G. Hendricks, J.E. Lazarus, E. Perlson, M.K. Gardner, D.J. Odde, Y.E. Goldman and E.L.F. Holzbaur, *Curr. Biol.* **22**, 632 (2012).